Original Research Article

Keller-Box Study on Casson Nano fluid Flow Over a slanted Permeable Surface with chemical reaction

Abstract

In this problem, examination of Casson Nanofluid boundary layer stream over linear slanted extending sheet by fusing the chemical reaction and heat generation impacts are under thought. Nanofluid demonstrate in this examination is developed on Buongiorno model for the warm efficiencies of the liquid streams in the presence of Brownian movements and thermophoresis impacts. The nonlinear issue for Casson Nanofluid stream over slanted channel is displayed to ponder the heat and mass exchange wonder by considering portant stream parameters to strengthened boundary layers. The governing nonlinear partial differential equations are decreased to nonlinear normal differential equations and afterward illustrated numerically by methods for the Keller-Box plot. An examination of the set up results in the absence of the joined impacts is performed with the accessible outcomes of Khan and Pop [1] and set up in a decent contract. Numerical and graphical outcomes are additionally exhibited in tables and graphs.

Keywords: Casson Nano fluid, Chemical reaction, Heat generation/absorption, inclined surface.

1 Introduction

In the prior couple of decades, quick advances in nanotechnology have brief creating of new age coolants called "Nano liquid". Nano liquids are potential heat trade fluids with improved thermo physical properties and heat trade execution can be associated in various gadgets for better exhibitions (for example imperativeness, heat trade and other performances).Nano liquids are structured by interfering with nanoparticles with typical sizes underneath 100 nm in ordinary heat trade liquids, for example, oil, water, and ethylene glycol. These are ebb and flow heat trade masters that trigger the thermal conductivity of the base liquids and an essential subject for specialists and scientists over the span of the most recent couple of years because of its varied planning and current applications Choi [2]. Eastman et al. [3] inspected in an investigation when nanoparticles are included base liquid (water) with volume portion 5% the thermal conductivity upgraded up to 60%. Moreover, Eastman et al. [3] announced that the thermal conductivity expanded up to 40% by including the copper nanoparticles with volume part 1% in the customary liquid ethylene glycol or oil. Buongiorno [4] has talked about in his investigation there are seven systems, which are imperative to upgrade the thermal conductivity of the base liquid. Among all these Brownian movement and thermophoresis are increasingly significant. Anwar et al. [5] studied the numerical study of micropolar nanofluid flow over a stretching sheet. Mitra [6] investigated computational modeling of nanofluid flow over a heated inclined plate. Khan et al. [7] illustrated the heat and mass transfer of MHD Jeffery nanofluid flow over

inclined sheet. Hatami et al. [8] discussed three dimensional steady nanofluid over an inclined disk. Govindrajan [9] investigated the nanofluid flow over a slanted sheet. Nanofluid flow with radiation effects on a slnted surface examined by Chakraborty [10]. Besides, similarity solution of nanofluid on permeable sheet studied by Ziaei-Rad et al. [11]. Thumma et al. [12] discussed the nanofluid flow on a slanted plate by incorporating the heat source.

Casson liquid is shear diminishing fluid which should have zero consistency at a boundless measure of shear and vast thickness at zero degree of shear, yield stress under which no stream occur. Shear diminishing states the answer of a liquid substance thickness when constrain connected. The instances of Casson liquid are jam, tomato glue, stock, thorough organic product fluids, and human blood and so on Kumar et al. [13]. Casson liquid stream assumes a key job in designing. Shaw et al. [14] discussed the effect of different parameters on Casson fluid stream over a plate with convective farthest point conditions at surface. Ali et al. [15] discussed the Casson fluid flow over a slanted sheet. Casson fluid flow over a slanted plate calculated by Vijayaragavan and Kavitha [16]. Shamshuddin et al. [17] numerically investigated the effect of chemical rection on Casson fluid flow on slanted plate. For more literature we can see [18-23].
The warmth and mass exchange with synthetic response over a slanted extending plate has achieved a significant intrigue as a result of its various applications in building. Anwar et al. [24] examined the MHD stagnation point flow of nanofluid stream over a sheet with within the sight of concoction response and warmth age. shit and Majee [25] expounded the impacts of compound response on magnetohydrodynmaic liquid stream over nonlinear extending slanted surface. Blended convection stream over a vertical plate by joining impacts of substance response and warmth age examined by Eid [26]. Malik [27] talked about MHD two dimensional stream over penetrable slanted surface with second order synthetic response. Jain and Bohra [28] examined the impact of compound response on three dimensional incompressible streams over a slanted surface. Heat and mass exchange MHD free convection stream over a slanted plate inspected by Sheri and Modugula [29].

2 Problem formulation

A steady, two dimensional boundary layer flow of Casson Nano fluid on a porous slanted linear enlarging plate with an angle γ is under account. The extending and free stream speeds are supposed to stand as, $u_w(x) = ax$ and $u_\infty(x) = 0$ respectively, here 'x' is the coordinate dignified along the extending surface and 'a' is a constant. The Brownian motion and thermophoresis properties are taken into account. The temperature T and Nano particle fraction C take the constant values T_w and C_w on the wall, on the other hand ambient forms for nanofluid temperature and mass fractions T_∞ and C_∞ are attained as y inclines to immensity shown in fig.1.

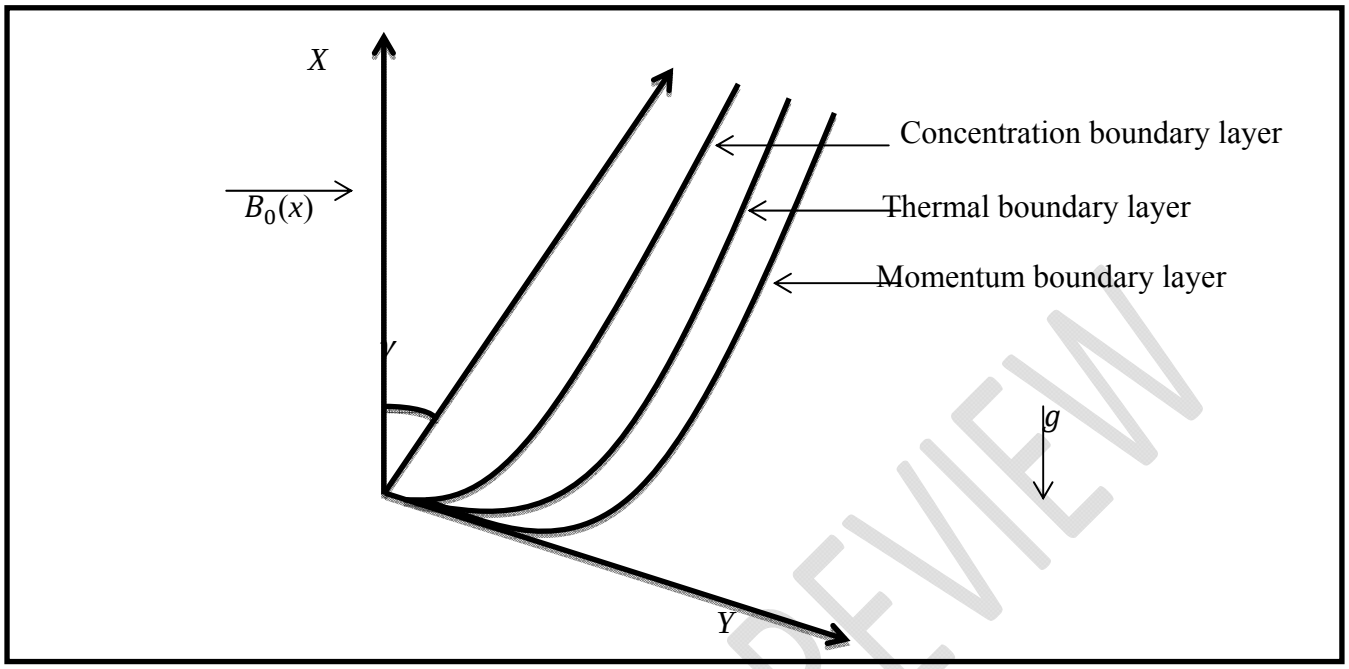

Fig.1. Physical geometry with coordinate system

$$\frac{\partial u}{\partial x}+\frac{\partial v}{\partial y}=0 \tag{1}$$

$$u\frac{\partial u}{\partial x}+v\frac{\partial u}{\partial y}=\nu(1+\frac{1}{\beta})\frac{\partial^2 u}{\partial y^2}+g[\beta_t(T-T_\infty)+\beta_c(C-C_\infty)]cos\gamma-\sigma{B_0}^2(x)u \tag{2}$$

$$u\frac{\partial T}{\partial x}+v\frac{\partial T}{\partial y}=\alpha\frac{\partial^2 T}{\partial y^2}+\tau\left[D_B\frac{\partial C}{\partial y}\frac{\partial T}{\partial y}+\frac{D_T}{T_\infty}\left(\frac{\partial T}{\partial y}\right)^2\right]+\frac{Q_0}{\delta C_p}(T-T_\infty) \tag{3}$$

$$u\frac{\partial C}{\partial x}+v\frac{\partial C}{\partial y}=D_B\frac{\partial^2 C}{\partial y^2}+\frac{D_T}{T_\infty}\frac{\partial^2 T}{\partial y^2}+R^*(C-C_\infty) \tag{4}$$

Where u and v are the components of velocity in x and y directions, respectively, g is the acceleration due to gravity, B_0 is the uniform magnetic field strength, σdenotes the electrical conductivity, μ is the viscosity, δ_f is the density of the improper liquid, δ_p denotes density of the nanoparticle, β_t is the factor of thermal extension, β_c denote the factor of concentration enlargement, D_B denote the Brownian diffusion factor and D_T denotes the thermophoresis diffusion factor, Q_0 is the heat generation or absorption coefficient, R^* is the chemical reaction coefficient,$(\delta c)_p$denotes the heat capacitance of the nanoparticles, $(\delta c)_f$ represents the heat capacitance of the improper liquid, thermal diffusivity parameter is denoted by $\alpha=\frac{k}{(\delta c)_f}$andthe

ratio between the effective heat capacity of the nanoparticle and heat capacity of the liquid is represented by $\tau = \frac{(\delta c)_p}{(\delta c)_f}$.

The subjected boundary conditions are

$$u = u_w(x) = ax, v = V_w, T = T_w, C = C_w \quad at \quad y = 0,$$

$$u \to u_\infty(x) = 0, v \to 0, T \to T_\infty, C \to C_\infty \quad at \quad y \to \infty, \tag{5}$$

Here we obtained nonlinear ordinary differential equations from nonlinear partial differential equations by using stream function $\psi = \psi(x, y)$ demarcated as

$$u = \frac{\partial \psi}{\partial y}, \; v = -\frac{\partial \psi}{\partial x}, \tag{6}$$

Where

equation (1) is fulfilled identically. The similarity transformations are demarcated as

$$u = axf'(\eta), v = -\sqrt{av} f(\eta), \eta = y\sqrt{\frac{a}{v}}$$

$$\theta(\eta) = \frac{T - T_\infty}{T_w - T_\infty}, \phi(\eta) = \frac{C - C_\infty}{C_w - C_\infty}, \tag{7}$$

On substituting equation (7), system of equations (2-4) reduces to the following nonlinear ordinary differential equations:

$$(1 + \tfrac{1}{\beta}) f''' + ff'' - f'^2 + (\lambda g + \delta q) cos\gamma - Mf' = 0 \tag{8}$$

$$\left(\tfrac{1}{Pr}\right)\theta'' + f\theta' + \lambda_1 \theta' + Nb\phi'\theta' + Nt\theta'^2 = 0 \tag{9}$$

$$\phi'' + Lef\phi' + Nt_b\theta'' - LeR\phi = 0 \tag{10}$$

Where

$$\lambda = \frac{Gr_x}{Re_x}, \delta = \frac{Gc}{Re_x}, M = \frac{\sigma B^2(x)}{a\rho}, Le = \frac{\nu}{D_B}, Pr = \frac{\nu}{\alpha}, N_b = \frac{\tau D_B (C_w - C_\infty)}{\nu}, N_t = \frac{\tau D_t (T_w - T_\infty)}{\nu T_\infty},$$

$$Gr_x = \frac{g\beta_t (T_w - T_\infty)x}{a\nu}, Re_x = \frac{u_w(x)x}{\nu}, Gc_x = \frac{g\beta_c (C_w - C_\infty)x}{a\nu}, \; Nt_b = \frac{N_t}{N_b}, \lambda_1 = \frac{Q_0}{a\rho c_p}, R = \frac{R^*}{a}, \tag{11}$$

Here, primes denotes the differentiation with respect to η, λ Buoyancy parameter, δ Solutal buoyancy parameter, M is the magnetic constraint, ν denotes the kinematic viscidness of the liquid, Pr denotes the Prandtl number, Le denotes the Lewis number, Chemical reaction parameter is denoted by R, λ_1 Heat generation or absorption parameter.

The equivalent boundary settings are converted to

$$f(\eta) = S, \quad f'(\eta) = 1, \ \theta(\eta) = 1, \ \phi(\eta) = 1 \quad at \ \eta = 0,$$
$$f'(\eta) \to 0, \quad \theta(\eta) \to 0, \ \phi(\eta) \to 0 \ as \ \eta \to \infty, \tag{12}$$

The skin friction, Sherwood number and Nusselt number for the current study are defined as

$$Nu_x = \frac{xq_w}{k(T_w - T_\infty)}, Sh_x = \frac{xq_m}{D_B(C_w - C_\infty)}, C_f = \frac{t_w}{{u_w}^2 \rho_f}, \tag{13}$$

The reduced Sherwood number $-\phi'(0)$, skin-friction coefficient $C_{fx}(0) = f''(0)$, and the reduced Nusselt number $-\theta(0)$, are demarcated as

$$-\theta'(0) = \frac{Nu_x}{\sqrt{Re_x}}, -\phi'(0) = \frac{Sh_x}{\sqrt{Re_x}}, C_{fx} = C_f\sqrt{Re_x}, \tag{14}$$

Where, $Re_x = \frac{u_w(x)x}{\nu}$ is the local Reynolds number

The converted nonlinear differential equations (8-10) with the boundary conditions (12) are elucidated by Keller box method consisting on the steps as, finite-differences technique, Newton's scheme and block elimination process clearly explained by Anwar et al. [30].

3 Results and discussion:

The transformed nonlinear ordinary differential equations (8-10) with boundary conditions (12) are solved via Killer-box method. For numerical result of physical parameters of our concern including Brownian motion parameter Nb, thermophoresis parameter Nt, Chemical reaction constraint R, magnetic factor M, buoyancy constraint λ, heat generation or absorption bound $\lambda 1$, solutal buoyancy constraint δ, inclination parameter γ, Casson fluid parameter β, Prandtl number Pr, Lewis number Le, and suction parameter S, several figures and tables are prepared. In Table 3.1, in the absence of buoyancy parameter λ, solutal buoyancy parameter δ, with γ = 90° when Casson constraint $\beta \to \infty$ outcomes for reduced Nusselt number $-\theta'(0)$, reduced Sherwood number $-\phi'(0)$ are equated with the existing outcomes of Khan and Pop [1]. The fallouts are established brilliant settlement. The effects of reduced Nusselt number $-\theta'(0)$, reduced Sherwood number $-\phi'(0)$ and skin friction coefficient $C_{fx}(0)$ against different values of involved physical parameters $Nb, \beta, Nt, R, M, \lambda 1, \lambda, \delta, \gamma, Pr, Le$, and S are shown in table 3.2. It is noted that $-\theta'(0)$ decreases for increasing the values of $Nb, \beta, \gamma, Nt, M, \lambda 1, Le, Pr, S$, and increased by increasing the numerical values of , R, λ, δ and for decreasing values of S. Moreover, it is observed that $-\phi'(0)$ enhanced with the larger values of $Nb, Pr, Nt, Le, \lambda 1, \lambda, \delta$, and for small values of S. Whereas, decreases for cumulative the values of R, γ,

171 $M$and S. On the other hand, $C_{fx}(0)$ surges with the increasing values of Nb, Le, M, β, $\lambda 1$, γ, and
172 for small values of S. Moreover, decreases with the increasing values of Nt, λ, δ, Pr, R, and S.

173

174 **Table 3.1:** Contrast of the reduced Nusselt number $-\theta'(0)$ and the reduced Sherwood number
175 $-\phi'(0)$ with M, δ, S, R, λ_1, $\lambda = 0$, Pr = Le = 10 and γ= 90° when $\beta \to \infty$.

Nb	***Nt***	Khan and Pop [1]		Current Outcomes	
		$-\theta'(0)$	$-\phi'(0)$	$-\theta'(0)$	$-\phi'(0)$
0.1	0.1	0.9524	2.1294	0.9524	2.1294
0.2	0.2	0.3654	2.5152	0.3654	2.5152
0.3	0.3	0.1355	2.6088	0.1355	2.6088
0.4	0.4	0.0495	2.6038	0.0495	2.6038
0.5	0.5	0.0179	2.5731	0.0179	2.5731

176

177

178

179

180

181

182

183

184

185

Table 3.2: outcomes of the reduced Nusselt number $-\theta'(0)$, the reduced Sherwood number $-\phi'(0)$ and the Skin-friction coefficient $C_{fx}(0)$.

Nb	*Nt*	Pr	*Le*	*M*	*β*	*R*	*λ 1*	*λ*	*δ*	*S*	*γ*	$-\theta'(0)$	$-\phi'(0)$	$C_{fx}(0)$
0.1	0.1	6.5	5.0	0.5	1.0	1.0	0.1	0.1	0.9	0.1	45^0	0.7385	0.7248	0.6709
0.3	0.1	6.5	5.0	0.5	1.0	1.0	0.1	0.1	0.9	0.1	45^0	0.2942	0.9897	0.6978
0.1	**0.3**	6.5	5.0	0.5	1.0	1.0	0.1	0.1	0.9	0.1	45^0	0.4591	0.9008	0.6139
0.1	0.1	**10.0**	5.0	0.5	1.0	1.0	0.1	0.1	0.9	0.1	45^0	0.6977	0.8104	0.6703
0.1	0.1	6.5	**10.0**	0.5	1.0	1.0	0.1	0.1	0.9	0.1	45^0	0.6220	1.5163	0.7203
0.1	0.1	6.5	5.0	**2.0**	1.0	1.0	0.1	0.1	0.9	0.1	45^0	0.6911	0.5356	1.0322
0.1	0.1	6.5	5.0	0.5	**5.0**	1.0	0.1	0.1	0.9	0.1	45^0	0.7183	0.6520	0.8109
0.1	0.1	6.5	5.0	0.5	1.0	**2.0**	0.1	0.1	0.9	0.1	45^0	1.1379	-2.3869	0.5423
0.1	0.1	6.5	5.0	0.5	1.0	1.0	**0.5**	0.1	0.9	0.1	45^0	-0.2881	1.5280	0.6821
0.1	0.1	6.5	5.0	0.5	1.0	1.0	0.1	**1.0**	0.9	0.1	45^0	0.7504	0.7570	0.5565
0.1	0.1	6.5	5.0	0.5	1.0	1.0	0.1	0.1	**3.0**	0.1	45^0	0.7736	0.8445	0.3438
0.1	0.1	6.5	5.0	0.5	1.0	1.0	0.1	0.1	0.9	**0.3**	45^0	0.3124	0.5246	0.6032
0.1	0.1	6.5	5.0	0.5	1.0	1.0	0.1	0.1	0.9	**0.0**	45^0	0.9988	0.8108	0.7060
0.1	0.1	6.5	5.0	0.5	1.0	1.0	1.0	1.0	1.0	**-0.3**	45^0	1.9229	1.0041	0.8114
0.1	0.1	6.5	5.0	0.5	1.0	1.0	1.0	1.0	1.0	0.1	$\mathbf{60^0}$	0.7334	0.7015	0.7191

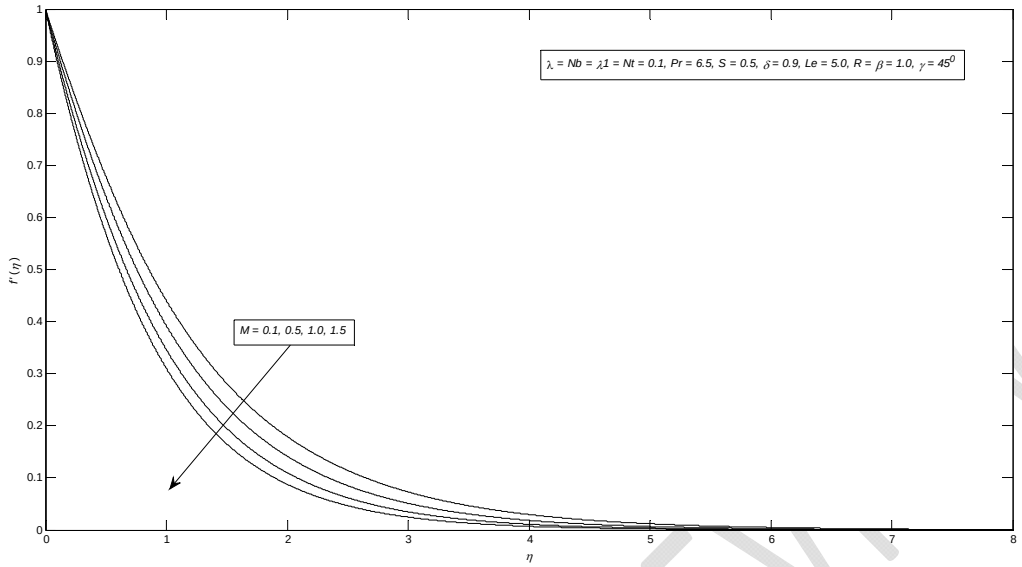

188

189 Fig. 2 velocity profile for several values of M.

190

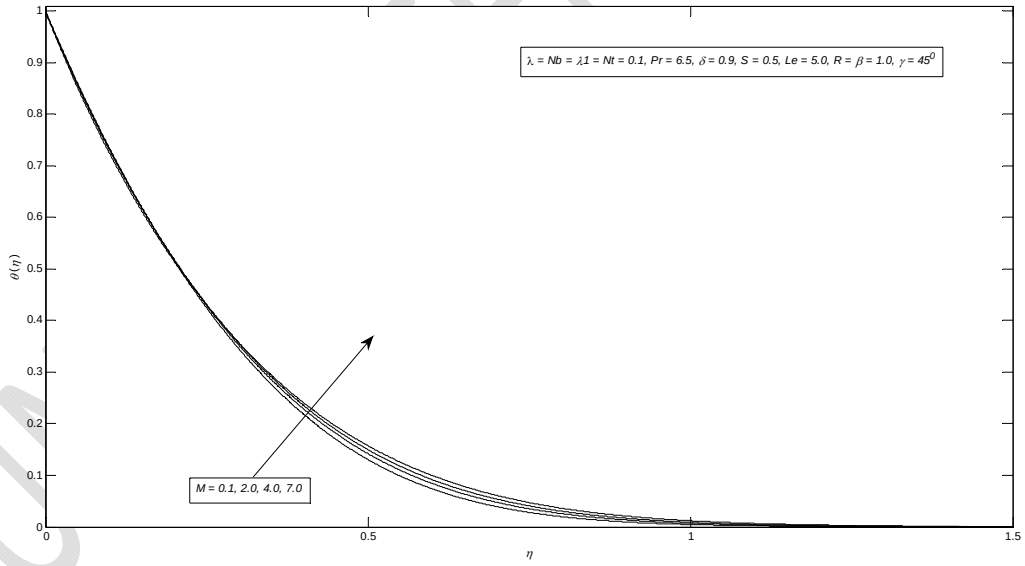

191

192 Fig. 3 temperature profile for several values of M.

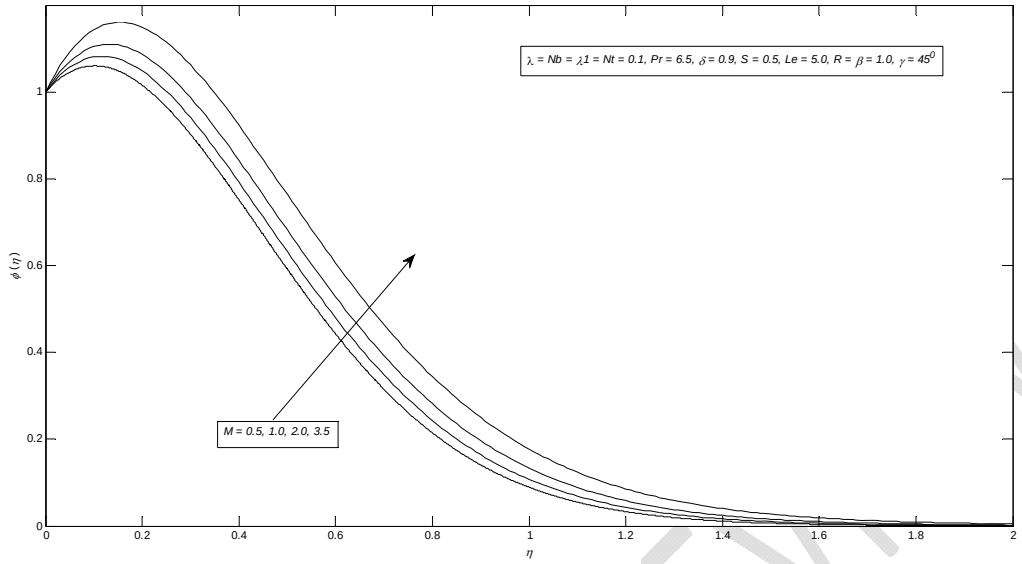

193

194 Fig. 4 concentration profile for several values of M.

195 Fig. 2 depicts the effect of magnetic field parameter on velocity profile. It is found that the
196 velocity profile retard as we upturn the magnetic field constraint M. It is due to the application of
197 magnetic field produces Lorentz force, by means slow down the speed of the fluid. Moreover,
198 figs. 3 and 4 present the temperature and concentration contours increase by enhancing the
199 values of M.

200

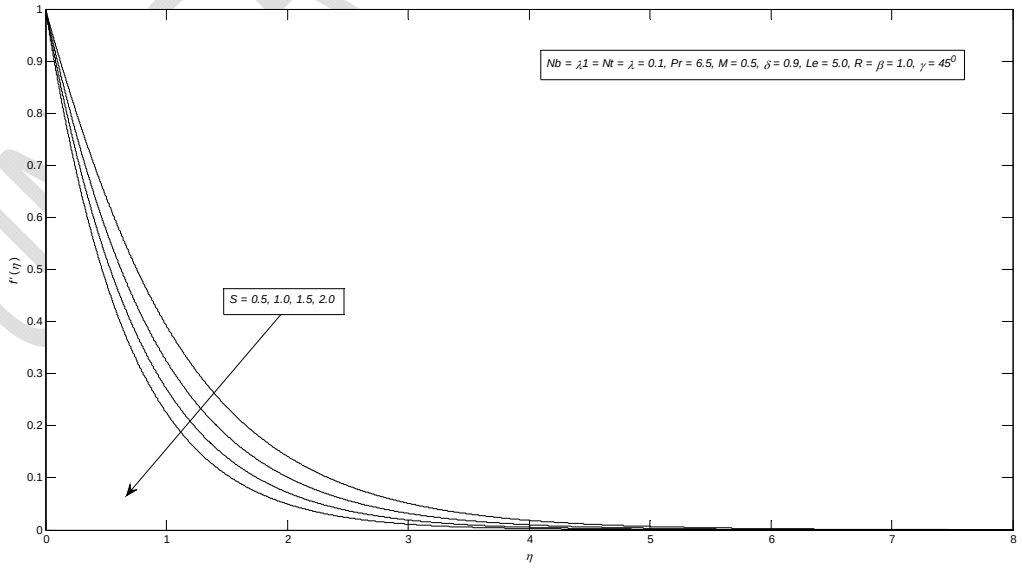

201
202 Fig. 5 velocity profile for several values of S.

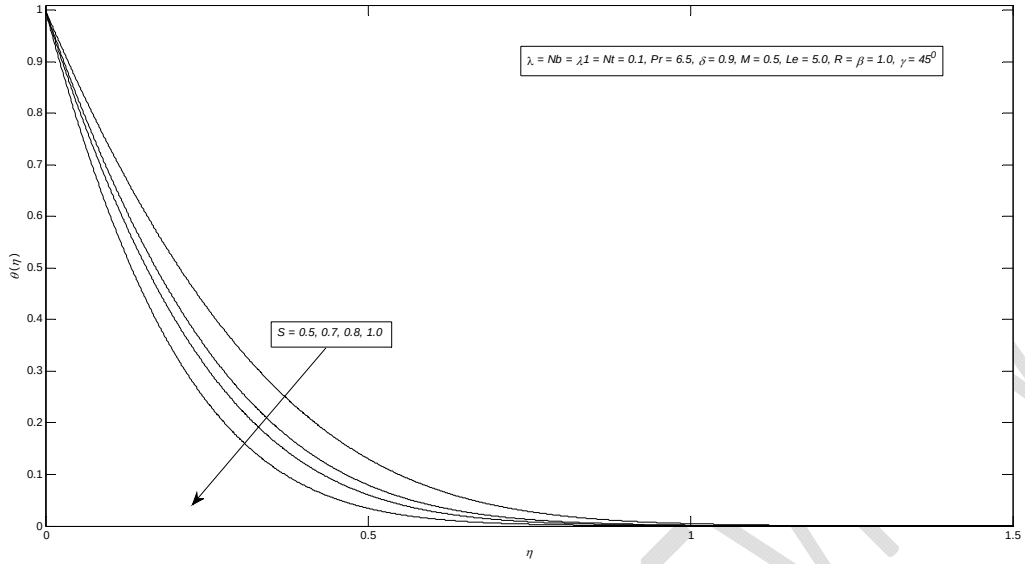

203

204 Fig. 6 temperature profile for several values of S.

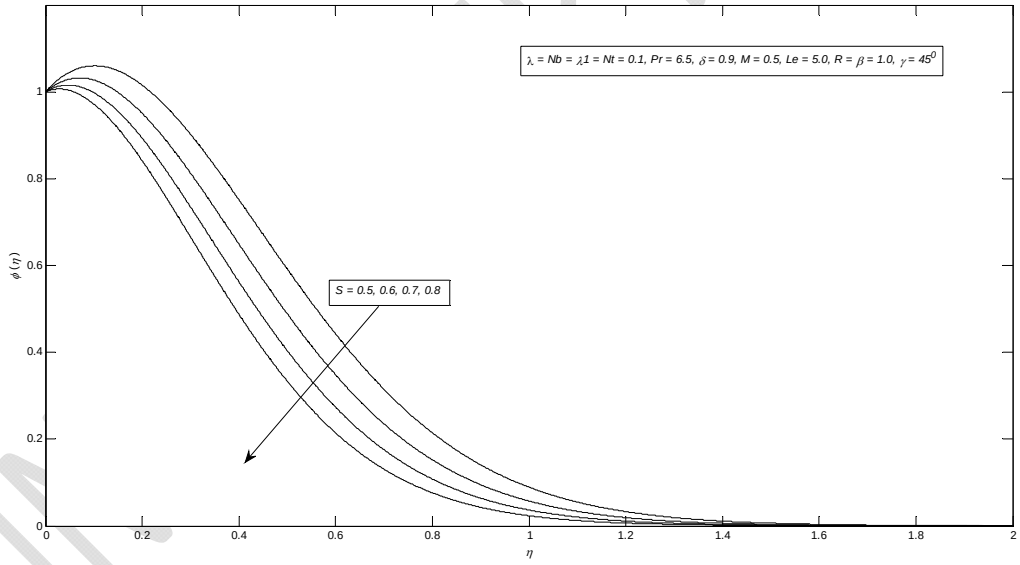

205

206 Fig. 7 concentration profile for several values of S.

207 The effects of suction parameter S on the velocity profile are shown in Fig. 5. It is perceived that
208 the velocity profile decline by growing the suction parameter signifying the normal fact that
209 suction steadies the boundary layer development due to which the creation of highest in the
210 velocity outline also drops. Besides, the same effect showed in the case of temperature profile
211 and concentration profile respectively in figs. 6 and 7.

212

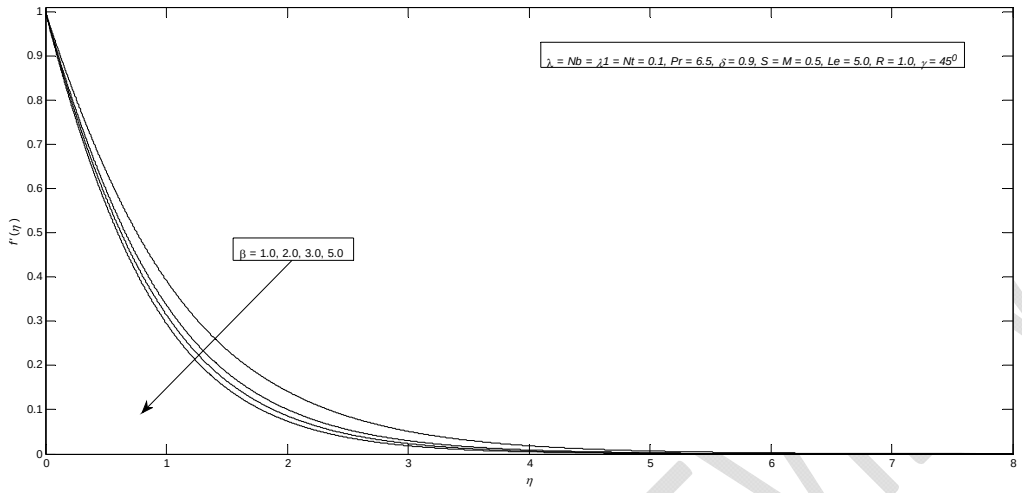

213

214 Fig. 8 velocity profile for several values of β.

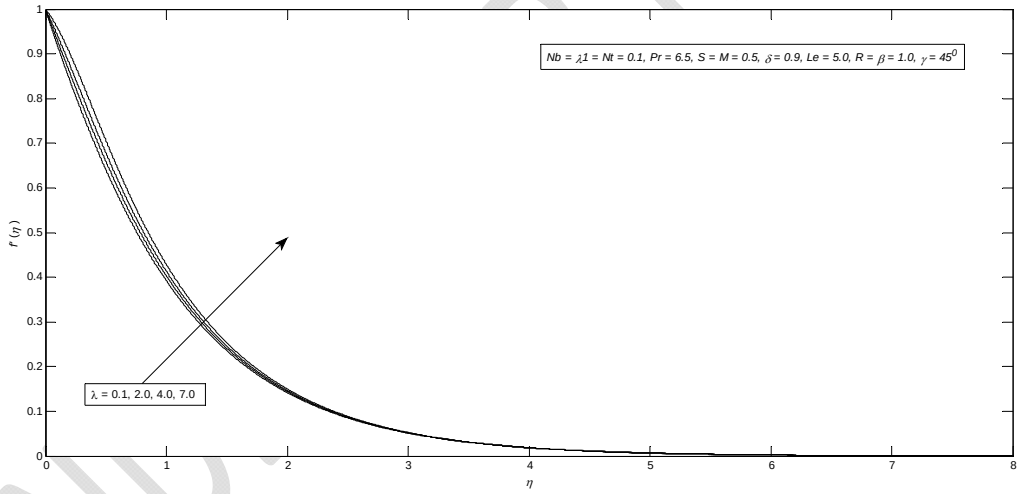

215

216 Fig. 9 velocity profile for several values of λ.

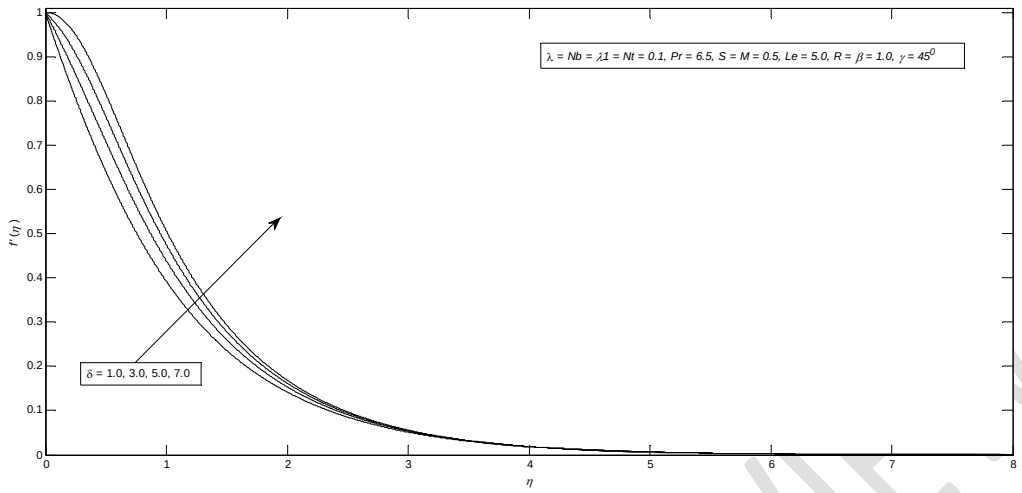

217

218 Fig. 10 velocity profile for several values of δ.

219 The outcome of Casson constraint on velocity factor is presented in Fig. 8. It is detected that for
220 different values of Casson parameter velocity profile decreases. The cause overdue this behavior
221 is that by growing the values of Casson parameter β increases the fluid viscosity i.e falling the
222 yield stress. Therefore, the momentum boundary layer thickness reduces. The impacts of
223 buoyancy factor are shown in Fig. 9. It is pragmatic that the velocity profile rise by improving
224 the buoyancy limit. Fig. 10 indicates that the velocity outline increases by enhancing the solutal
225 buoyancy factor.

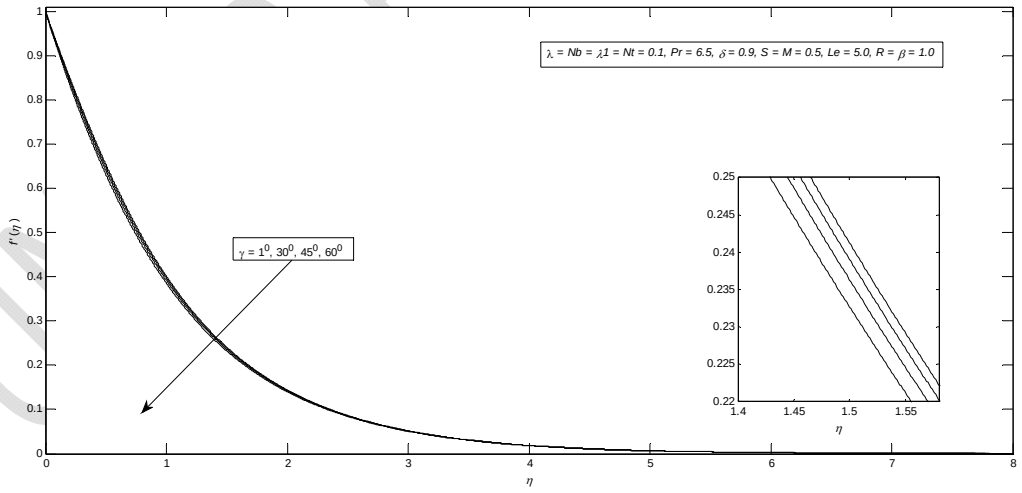

226

227 Fig. 11 velocity profile for several values of γ.

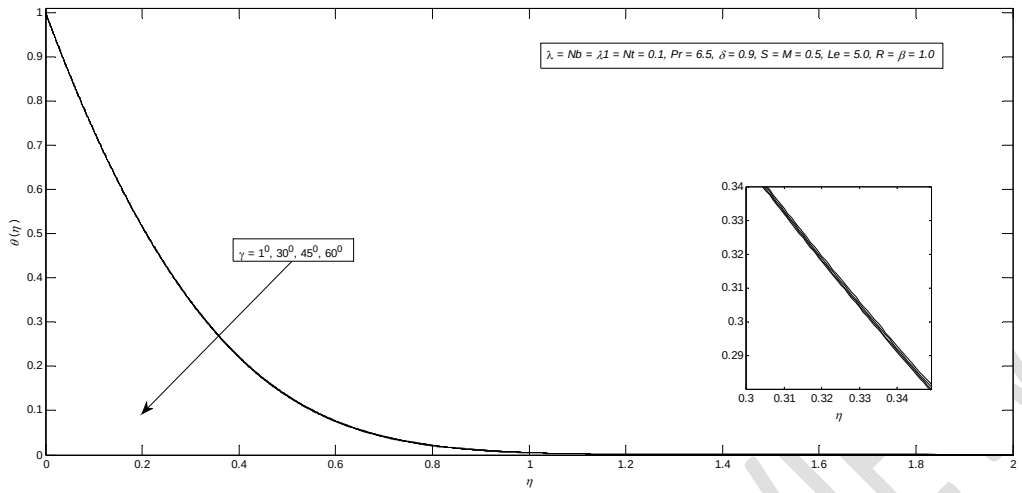

228

229 Fig. 12 temperature profile for several values of γ.

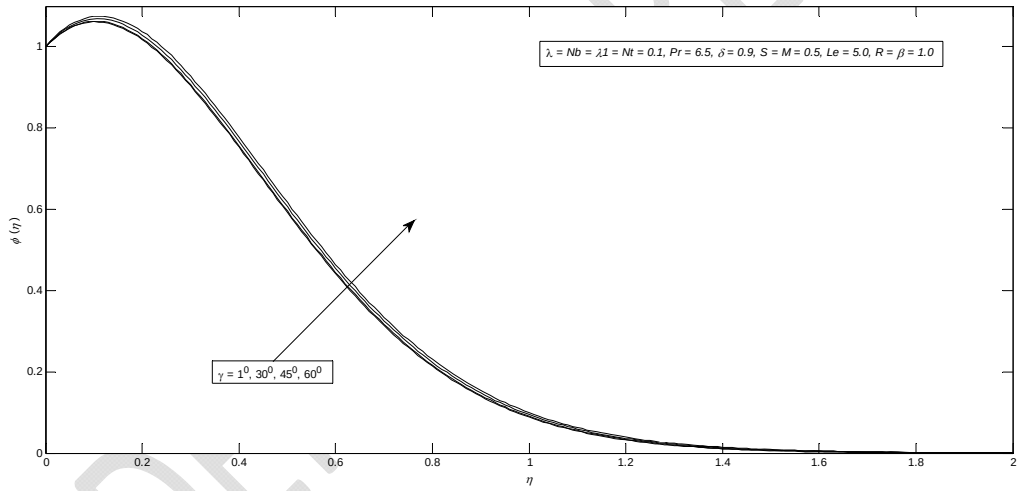

230

231 Fig. 13 concentration profile for several values of γ.

232 Fig. 11 indicates that the velocity profile decelerated by enhancing the values of inclination
233 parameter γ. This is because of enhancing the value of inclination parameter; retard the strength
234 of the bouncy force by a factor $cos\gamma$ because of the thermal variation. Also we found that the
235 influence of the bouncy force (which is highest for $\gamma = 0$) exceeds the main stream velocity
236 significantly. The same impact indicates in Fig. 12 for temperature profile but opposite impact
237 presents in the case of concentration profile in fig. 13.

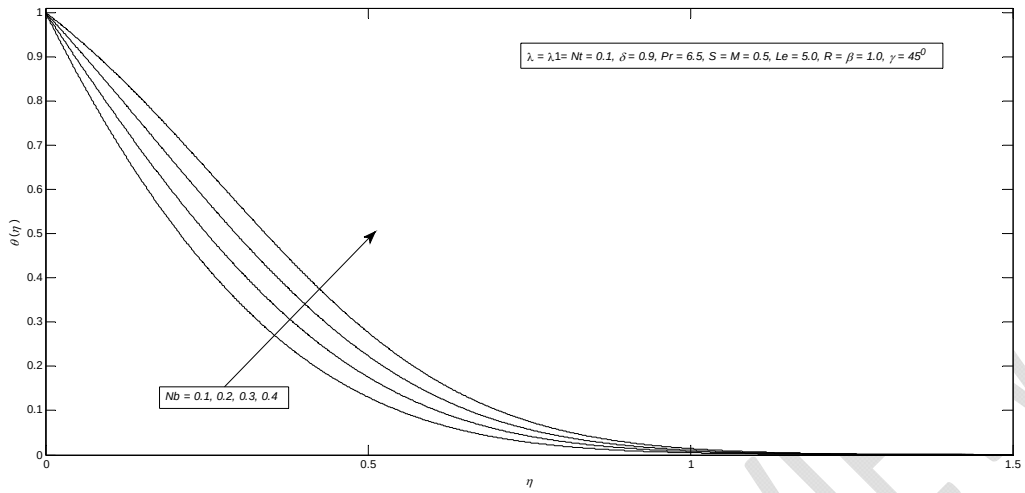

238
239 Fig. 14 temperature profile for several values of Nb.

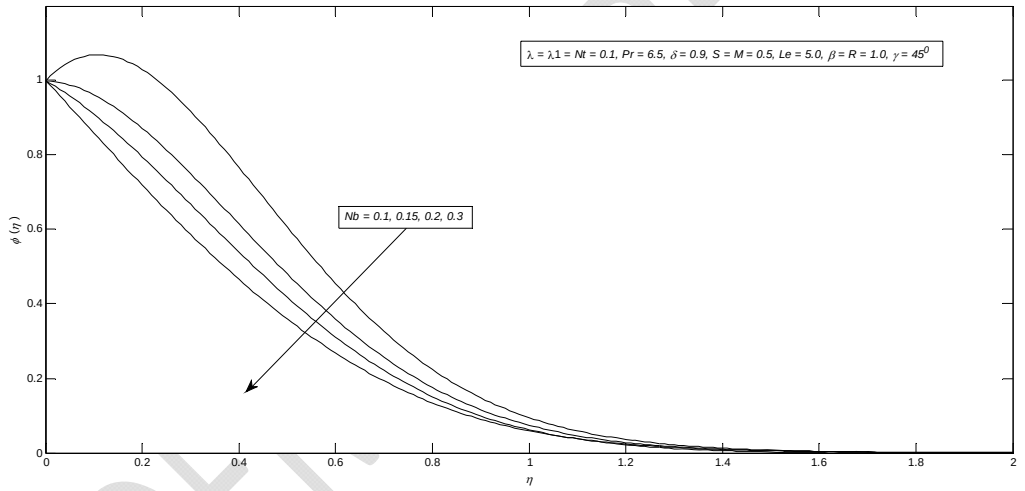

240

241 Fig. 15 concentration profile for several values of Nb.

242

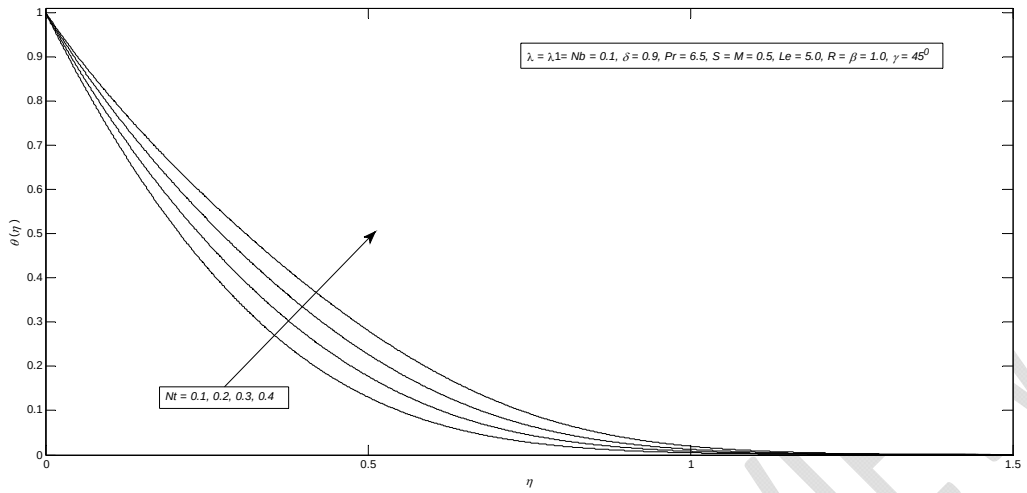

243

244 Fig. 16 temperature profile for several values of Nt.

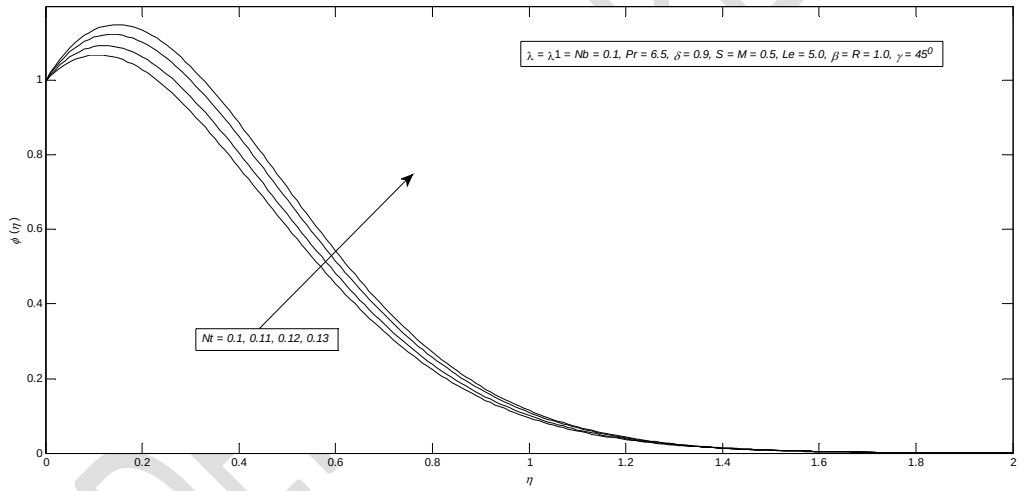

245

246 Fig. 17 concentration profile for several values of Nt.

247 Figures 14 and15 indicate the effect of Brownian cue on the temperature and concentration
248 outlines. The temperature contour enlarges by enhancing the Brownian motion. Moreover,
249 contrary style is seen beside the concentration outlines. Substantially, the enlargement in
250 Brownian movement factor supports to heat up the boundary layer which inclines to travel
251 nanoparticles from the extending sheet to the motionless liquid. Therefore the concentration
252 nanoparticle moderates. Moreover, figs 16 and 17 specify the effects of thermophoresis
253 parameter on temperature and concentration contours. It is found that mutually temperature and
254 concentration profiles are increases for large values of thermophoresis parameter Nt.

255

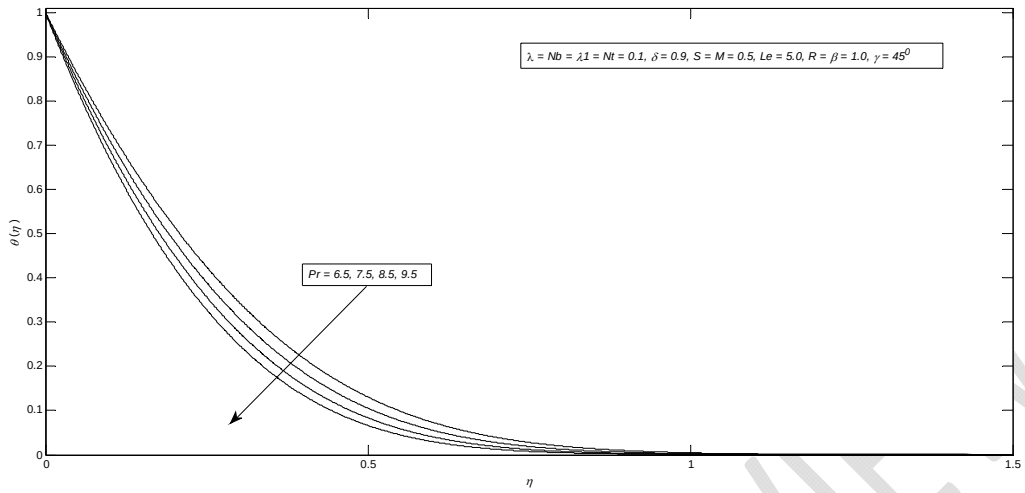

256

257 Fig. 18 temperature profile for several values of Pr.

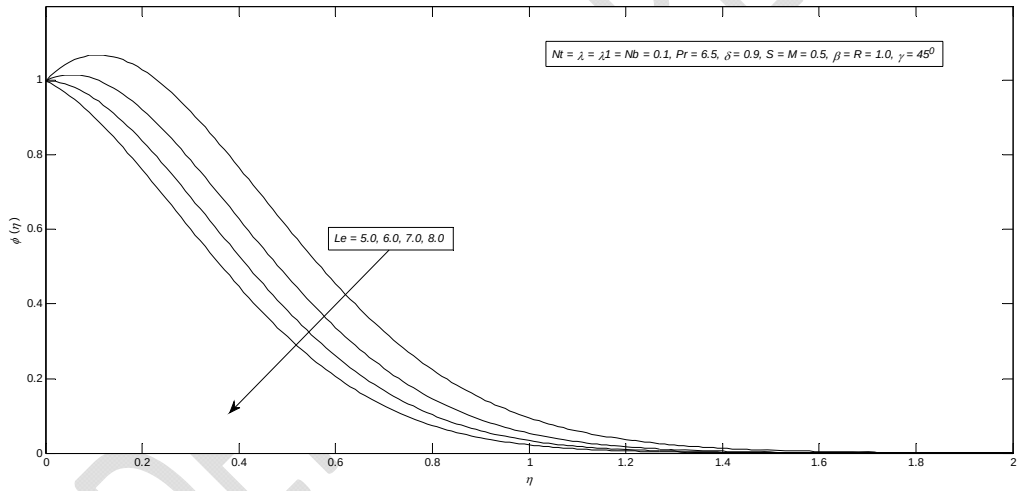

258

259 Fig. 19 concentration profile for several values of Le.

260 Figs. 18 and 19 depict the effect of Prandtl number Pr on temperature and Lewis number Le on
261 concentration profile. It indicates that the temperature profile decrease for large values of Prandtl
262 number. The boundary layer thickness shortens by enhancing the values of Prandtl number.
263 Moreover, the concentration profile decrease for higher values of Lewis number Le which shows
264 Lewis number reduces the boundary layer thickness.

265

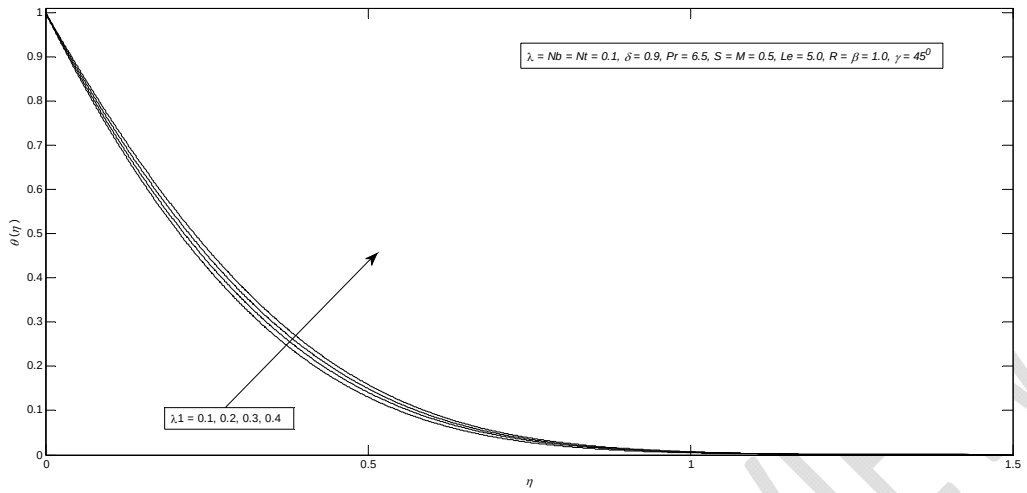

Fig. 20 temperature profile for several values of λ_1.

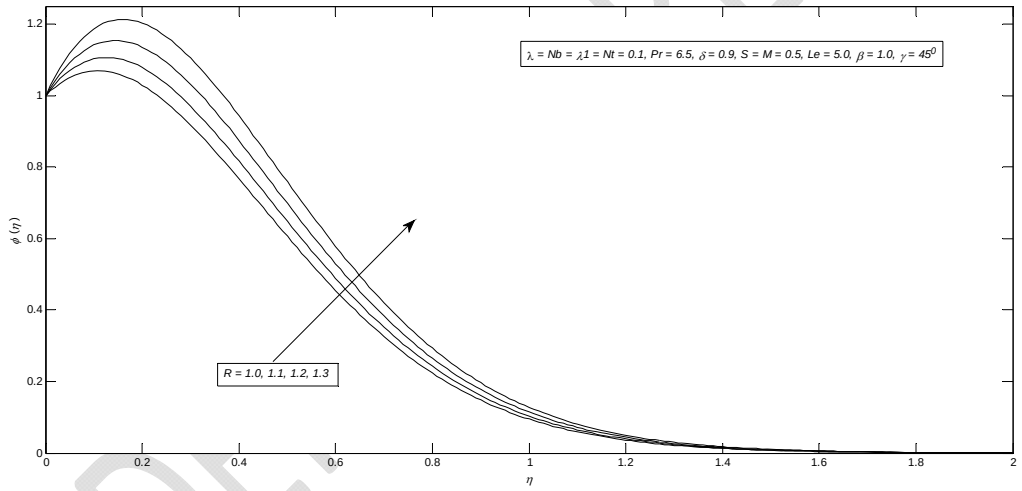

Fig. 21 concentration profile for several value of R.

Fig. 20 and 21 presented the effect of heat generation on temperature and chemical reaction on concentration outline. It is noted that the temperature and concentration contour upsurge by growing the values of heat generation constraint λ_1 and chemical reaction constraint R. The velocity of the liquid enhance by increasing the values of heat generation, due to which heat generate in the flow region and the temperature increase with in the thermal boundary layer.

4 Conclusions

In progress problem is explored the heat and mass exchange of Casson nanofluid flow above porous linear slanted extending sheet. It is noted that $-\theta'(0)$ declines for growing the values of $Nb, \beta, \gamma,\ Nt, M, \lambda 1, Le, Pr, S$, and enlarged by growing the numerical values of , R, λ, δ and for lessening values of S. Moreover, it is observed that $-\phi'(0)$ enhanced with the superior values of $Nb, Pr, Nt, Le, \lambda 1, \lambda, \delta$, and for lesser values of S. Whereas, drops for swelling the values of R, $\gamma, M$and S. On the other hand, $C_{fx}(0)$ upsurges with the cumulative values of Nb, Le, M, β, $\lambda 1$, γ, and for lesser values of S. Moreover, drops with the growing values of Nt, λ, δ, Pr, R, and S.

References

[1] Khan, W. A., & Pop, I. (2010). Boundary-layer flow of a nanofluid past a stretching sheet. *International Journal of Heat and Mass Transfer*, *53*(11), 2477–2483.

[2] Choi, S. U. S., Singer, D. A., & Wang, H. P. (1995). Developments and applications of non-Newtonian flows. *ASME FED*, *66*, 99–105.

[3] Eastman, J. A., Choi, U. S., Li, S., Thompson, L. J., & Lee, S. (1996). Enhanced thermal conductivity through the development of nanofluids. *MRS Online Proceedings Library Archive*, *457*.

[4] Buongiorno, J. (2006). Convective transport in nanofluids. *Journal of Heat Transfer*, *128*(3), 240–250.

[5] Anwar, M. I., Shafie, S., Hayat, T., Shehzad, S. A., & Salleh, M. Z. (2017). Numerical study for MHD stagnation-point flow of a micropolar nanofluid towards a stretching sheet. *Journal of the Brazilian Society of Mechanical Sciences and Engineering*, *39*(1), 89–100.

[6**]** Mitra, A. (2018). Computational Modelling of Boundary-Layer Flow of a Nano fluid Over a Convective Heated Inclined Plate. *JOURNAL OF MECHANICS OF CONTINUA AND MATHEMATICAL SCIENCES*, *13*(2), 88-94.

[7**]** Khan, M., Shahid, A., Malik, M. Y., & Salahuddin, T. (2018). Thermal and concentration diffusion in Jeffery nanofluid flow over an inclined stretching sheet: A generalized Fourier's and Fick's perspective. *Journal of Molecular Liquids*, *251*, 7–14.

[8**]** Hatami, M., Jing, D., & Yousif, M. A. (2018). Three-dimensional analysis of condensation nanofluid film on an inclined rotating disk by efficient analytical methods. *Arab Journal of Basic and Applied Sciences*, *25*(1), 28–37.

[9] Govindarajan, A. (2018, April). Radiative fluid flow of a nanofluid over an inclined plate with non-uniform surface temperature. In *Journal of Physics: Conference Series* (Vol. 1000, No. 1, p. 012173). IOP Publishing.

[10] Chakraborty, T., Das, K., & Kundu, P. K. (2017). Ag-water nanofluid flow over an inclined porous plate embedded in a non-Darcy porous medium due to solar radiation. *Journal of Mechanical Science and Technology*, *31*(5), 2443-2449.

[11] Ziaei-Rad, M., Kasaeipoor, A., Rashidi, M. M., & Lorenzini, G. (2017). A similarity solution for mixed-convection boundary layer nanofluid flow on an inclined permeable surface. *Journal of Thermal Science and Engineering Applications*, *9*(2), 021015.

[12] Thumma, T., Bég, O. A., & Sheri, S. R. (2017). Finite element computation of magnetohydrodynamic nanofluid convection from an oscillating inclined plate with radiative flux, heat source and variable temperature effects. *Proceedings of the Institution of Mechanical Engineers, Part N: Journal of Nanomaterials, Nanoengineering and Nanosystems*, *231*(4), 179-194.

[13] Kumar, M. S., Sandeep, N., Kumar, B. R., & Saleem, S. (2017). A comparative study of chemically reacting 2D flow of Casson and Maxwell fluids. *Alexandria Engineering Journal*.

[14] Shaw, S., Mahanta, G., & Sibanda, P. (2016). Non-linear thermal convection in a Casson fluid flow over a horizontal plate with convective boundary condition. *Alexandria Engineering Journal*, *55*(2), 1295–1304.

[15] Ali, M., Aruna, G., & Raju, R. S. (2018). MHD Boundary Layer Casson Fluid Flow Over a Vertically Inclined Plate: Grid Study and Convergence Analysis of Finite Element Technique. *Journal of Nanofluids*, *7*(6), 1195-1207.

[16] Vijayaragavan, R., & Kavitha, M. A. (2018). Heat and Mass Transfer in Unsteady MHD Casson Fluid Flow past an Inclined Plate with Thermal Radiation and Heat source/sink. *Research Journal of Engineering and Technology*, *9*(2), 214–233.

[17] Shamshuddin, M. D., Mishra, S. R., & Thumma, T. (2019). Chemically Reacting Radiative Casson Fluid Over an Inclined Porous Plate: A Numerical Study. In *Numerical Heat Transfer and Fluid Flow* (pp. 469-479). Springer, Singapore.

[18] Manideep, P., Raju, R. S., Rao, T. S. N., & Reddy, G. J. (2018, May). Unsteady MHD free convection flow of casson fluid over an inclined vertical plate embedded in a porous media. In *AIP Conference Proceedings* (Vol. 1953, No. 1, p. 140038). AIP Publishing.

[19] Raju, R. S., Reddy, B. M., & Reddy, G. J. (2017). Finite element solutions of free convective Casson fluid flow past a vertically inclined plate submitted in magnetic field in presence of heat and mass transfer. *International Journal for Computational Methods in Engineering Science and Mechanics*, *18*(4-5), 250-265.

[20] Vijayaragavan, R., & Kavitha, M. A. (2018). Heat and Mass Transfer in Unsteady MHD Casson Fluid Flow past an Inclined Plate with Thermal Radiation and Heat source/sink. *Research Journal of Engineering and Technology*, *9*(2), 214-223.

[21] Prasad, D. K., Chaitanya, G. K., & Raju, R. S. (2018, May). Role of casson fluid on MHD natural convective flow towards vertically inclined plate with hall current. In *AIP Conference Proceedings* (Vol. 1953, No. 1, p. 140073). AIP Publishing.

[22] Koriko, O. K., Oreyeni, T., Omowaye, A. J., & Animasaun, I. L. (2016). Homotopy analysis of MHD free convective micropolar fluid flow along a vertical surface embedded in non-darcian thermally-stratified medium. *Open Journal of Fluid Dynamics*, *6*(3), 198–221.

[23] Jain, S., & Parmar, A. (2018). Multiple slip effects on inclined MHD Casson fluid flow over a permeable stretching surface and a melting surface. *INTERNATIONAL JOURNAL OF HEAT AND TECHNOLOGY*, *36*(2), 585-594.

[24] Anwar, I., Rahman, A., Kasim, M., Ismail, Z., Salleh, M. Z., & Shafie, S. (2013). Chemical Reaction and Uniform Heat Generation or Absorption Effects on MHD Stagnation-Point Flow of a Nanofluid over a Porous Sheet, *24*(10), 1390–1398. https://doi.org/10.5829/idosi.wasj.2013.24.10.1307

[25] Shit, G. C., & Majee, S. (2014). Hydromagnetic Flow over an Inclined Non-Linear Stretching Sheet with Variable Viscosity in the Presence of Thermal Radiation and Chemical Reaction. *Journal of Applied Fluid Mechanics*, *7*(2).

[26] Eid, M. R. (2016). Chemical reaction effect on MHD boundary-layer fl ow of two-phase nano fl uid model over an exponentially stretching sheet with a heat generation. *Journal of Molecular Liquids*, *220*, 718–725. https://doi.org/10.1016/j.molliq.2016.05.005

[27] Malik, M. Y. (2016). Effects of Second Order Chemical Reaction on MHD Free Convection Dissipative Fluid Flow past an Inclined Porous Surface by way of Heat Generation : A Lie Group Analysis 1 Introduction 2 Flow analysis, *45*(2), 35–45.

[28] Bohra, S. (2017). Heat and mass transfer over a three-dimensional inclined non-linear stretching sheet with convective boundary conditions. *Indian Journal of Pure & Applied Physics (IJPAP)*, *55*(12), 847-856.

[29] Sheri, S. R., & Modugula, P. (2017). Thermal-diffusion and diffusion-thermo effects on MHD flow through porous medium past an exponentially accelerated inclined plate with variable temperature. *ARPN Journal of Engineering and Applied Sciences*, *12*(19), 5518–5526. https://doi.org/10.1016/j.asej.2015.08.014

[30] Anwar, M. I., Shafie, S., Hayat, T., Shehzad, S. A., & Salleh, M. Z. (2017). Numerical study for MHD stagnation-point flow of a micropolar nanofluid towards a stretching sheet. *Journal of the Brazilian Society of Mechanical Sciences and Engineering*, *39*(1), 89–100. https://doi.org/10.1007/s40430-016-0610-y